# The Measurement of Thermal Stress Distributions Along the Flow Path in Injection-Molded Flat Plates

C. H. V. HASTENBERG,* P. C. WILDERVANCK, *and* A. J. H. LEENEN

*Philips Competence Centre Plastics B.V.*
*5600 MD Eindhoven, The Netherlands*

*and*

G. G. J. SCHENNINK**

*University of Twente*
*The Netherlands*

Internal stresses in injection-molded parts are the result of thermal, flow, and pressure histories. Internal stresses can be roughly divided into thermal and flow-induced stresses. In this paper, a modified layer-removal method is presented to determine thermal stress distributions in injection-molded flat plates. With this method, the curvature of a rectangular specimen is determined after the removal of a layer from one surface. This curvature is converted into a stress via a mathematical relation, originally derived by Treuting and Read. By determining the local curvatures after successive layer removals, stress distributions along the flow path were obtained within a single specimen. Validation of this modified layer-removal method is described. A good reproductibility was obtained. The method can be regarded as semi-quantitative. Flat plates were injection-molded from three amorphous polymers: polystyrene, polycarbonate, and a polyphenylene ether/high-impact polystyrene blend. In general, the flat-plate cross-section shows a three-region stress distribution with a tensile stress region both at the surface and in the core of the flat plate and an intermediate region with compressive stresses. The modified layer-removal method was used to determine influences of mold temperature, annealing treatment, and pressure history on the thermal stress distributions. Increasing mold temperature results in a decreasing overall stress level, while the compressive stress region shifts to the surface. An annealing treatment significantly reduces the overall stress level, without affecting the stress pattern. Stress distributions along the flow path were influenced by the varying pressure histories from the entrance to the end of the mold cavity. The various features of the stress profiles are explained by the influence of the pressure decay rate in the injection-molding process.

## INTRODUCTION

Internal or residual stresses are a principal cause of dimensional and shape inaccuracies (e.g., shrinkage and warpage) observed in injection-molded plastic parts (1). Moreover, internal stresses are supposed to be responsible for environmental stress cracking, an important failure mechanism for plastic parts (2). Consequently, internal stresses are of great practical importance.

These internal stresses can be attributed to two main sources. The first is the shear and normal stresses that develop during the nonisothermal flow of a polymer melt in the mold cavity during filling and packing. These stresses do not completely relax but rather are frozen in because of rapidly increasing relaxation times during cooling. Such stresses

*To Whom correspondence should be addressed.
** Present address: Eindhoven University of Technology, The Netherlands.

are referred to as (residual) flow-induced stresses, introducing molecular orientation (3–5).

The second type of internal stress is due to rapid inhomogeneous cooling of a polymer melt. During initial cooling, surface layers will stiffen sooner than the core region. The subsequent solidification and thermal contraction of the core will produce residual thermal stresses (6). The free-quench models of Struik (6) and Wimberger-Friedl and Hendriks (7) are based on this type of internal stress development. These models, which only account for the thermal history of the specimen, predict more or less parabolic stress distributions with compressive stresses at the surface and tensile stresses in the core. However, in injection molding the quench conditions are different from a free quench. Therefore, in recent years attempts have been made to predict the development of thermal stresses in injection-molded parts by numerical simulation (5, 8–10). Besides the influence of thermal history, these models account for melt pressure history and mechanical constraints, i.e., interaction between polymer melt and mold during cooling.

Predicted thermal stress distributions differ substantially from a parabolic stress distribution. The most striking feature is a large stress gradient in the surface region. In most cases a surface tensile stress is predicted. Up till now, however, there has been no rigorous verification by experimentally obtained thermal stress distributions. Stresses in the surface region are especially difficult to determine, although Zoetelief, *et al.* (11) have made a first approach.

To determine internal stresses in injection-molded flat plates, the layer-removal method is frequently used (12–14). Since flow stresses are at least one order of magnitude smaller than thermal stresses, their influence on the overall internal stress level is negligible (5). Consequently, the stresses as measured with the layer-removal method are mainly of thermal origin.

With this method, thin layers of uniform thickness are removed from one surface of a rectangular specimen, thus upsetting the residual stress distribution in the specimen. To re-establish equilibrium, the specimen ideally warps to the shape of a circular arc. Curvature as a function of the remaining layer thickness is determined, and the thermal stresses can be calculated using the Treuting and Read relation (15). Usually, the layer-removal method is applied to a rectangular specimen, which is assumed to have no variation of the stress in the plane of the specimen but only through the thickness (15).

In the injection-molding process, the build-up and distribution of thermal stresses is governed largely by the various process parameters, which vary in the plane of the plate. For the assessment of the varying stress level along the flow path, different specimens have to be isolated at distinct places along this path (12, 14).

In this paper, the relation between process parameters and thermal stress development in plastic parts will be addressed, with emphasis on a modified layer-removal method to determine the stress distribution along the flow path within a single specimen.

## EXPERIMENTAL

Flat plates (80 × 35 × 2 mm) were injection molded on a servo-controlled injection-molding machine (Arburg Allrounder 270-90-350 with a Philips PMC 1000 control system) with a clamping force of 350 kN. The materials used were polystyrene (PS), polycarbonate (PC), and a blend of polyphenylene ether and high-impact polystyrene (PPE-HIPS). The specifications of these materials are summarized in *Table 1*. The mold was designed for optimal mechanical and thermal behavior, as described in detail elsewhere (4). The trapezoidal gate has a varying depth in order to realize a perfect linear flow front at the entrance of the rectangular part of the mold. The position of the flow front was detected by two optical sensors. The thermal behavior was measured by several thermocouples located in the mold at a distance of 1 mm from the cavity. Along the sprue and the product, four cavity pressure transducers recorded the time- and place-dependent pressure behavior. The plate and the location of the pressure transducers are schematically shown in *Fig. 1*.

The various processing parameters used in this study are summarized in *Table 2*.

After injection molding, the flat plates were stored for about one week at 23°C and 50% RH. Specimens with dimensions 70 × 18 × 2 mm were then cut with a circular saw from the center of the rectangular part (80 × 35 × 2 mm) of the original plate. From this specimen, layers were successively removed using a milling machine (Reichert-Jung Ultrafräse) with a diamond cutter. The speed of rotation was 1250 rpm. During milling, the specimens were held flat by a vacuum jig or by double-sided adhesive tape.

Within 6 min after each layer removal, the deflection of the surface opposite to the one from which the layer was removed was measured with a Perthen

**Table 1. Material Properties.**

| Material | Type | Supplier | Glass Transition Temperature (°C)[a] | Flexural Modulus (MPa) |
|---|---|---|---|---|
| PS | Styron 678E | Dow Chemical | 90 | 3400 |
| PC | Makrolon CD2000 | Bayer | 143 | 2500 |
| PPE-HIPS | Noryl SE-1 | General Electric | 137 | 2600 |

[a] Measured by differential scanning calorimetry.

Formtester MMR4 provided with a mechanical sensor. During this measurement, the specimen was supported by two cylindrical steel rods with a diameter of 5 mm at a distance of 35 mm, schematically shown in *Fig. 2*. A measuring force of 0.005 N was found to be sufficiently low to prevent additional bending of the specimen. Profile data were stored in a computer, so that they were available for further manipulation. Over a distance of 70 mm, 1500 measuring points were recorded.

By measuring in this way, it is possible to determine the curvature at an arbitrary position along the flow path. In the presented investigation, the total profile was subdivided into three segments with segment 1 nearest to the gate. A typical example of a measured profile is shown in *Fig. 3*. Each segment is regarded as a separate curved part, assuming a constant curvature within that segment. So the curvature $K$ can be calculated from

$$\kappa = \frac{8\phi}{L^2 + 4\phi^2} \qquad (1)$$

where $L$ is the length of the chord and $\phi$ the deflection (distance from chord to arc in the midpoint of the chord) (see *Fig. 3*). A curvature concave with respect to the surface from which a layer was removed is assigned a positive sign.

## VALIDATION OF THE LAYER-REMOVAL METHOD

In order to obtain reliable results, several aspects of the layer-removal method were investigated and are presented in summarized form here.

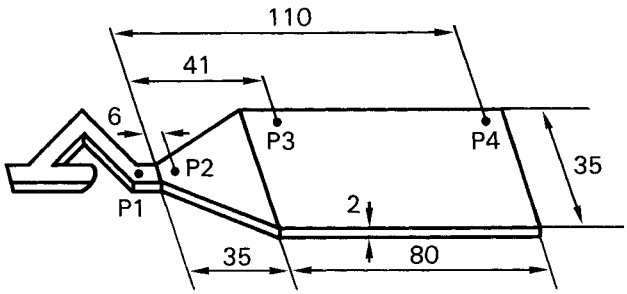


*Fig. 1. Flat-plate configuration and location of pressure tranducers P1 to P4 (dimensions in mm). The first (P1) is located at the end of the runner; the other transducers (P2, P3, P4) are located downstream from the entrance of the plate.*

- Its reproductibility was checked by removing layers from different samples of series No23 and measuring the resulting deflection of segments 1 and 3, as shown in *Fig. 3*. The results are shown in *Table 3*, indicating a good reproductibility.
- The possible influence of machining procedures was studied by using compression-molded PS plates, which were treated for 1 h at 80°C, i.e., 10°C below the glass transition temperature $T_g$, in order to remove thermal stresses. After successive layer removals, the specimens showed essentially no deflection, indicating the absence of any stresses introduced by machining.
- An additional investigation included verification of an experiment described by Isayev and Crouthamel (12), using compression-molded PS plates with a thickness of 2.55 mm, free-quenched from a glycerine bath after 10 min at 130°C in water of 23°C. The reader is referred to Ref. 12 for a detailed description of the original experiment. An excellent agreement with the original results was found, as shown in *Fig. 4*.

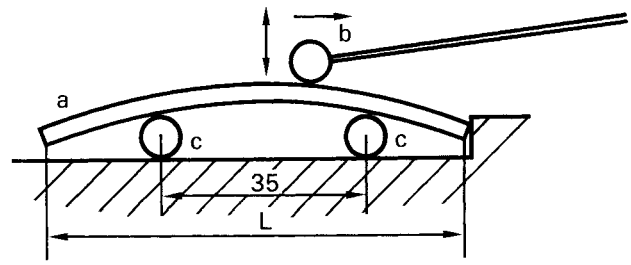


*Fig. 2. Configuration for deflection measurement. Layers are successively removed from the lower surface of the specimen. a: specimen; b: mechanical sensor; c: steel rod. L: length of chord.*

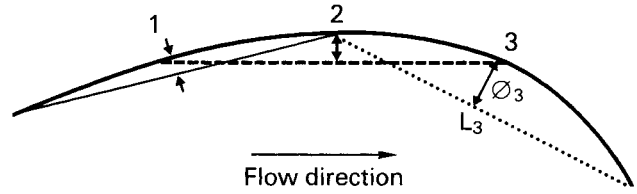


*Fig. 3. Typical example of measured deflection profile, divided into 3 segments. Solid line: chord of segment 1. Dashed line: chord of segment 2. Dotted line: chord of segment 3. $\phi_3$: deflection for segment 3. $L_3$: length of chord for segment 3.*

**Table 2. Process Parameters (Set Points).**

| Series | Material | Mold Temperature (°C) | Melt Temperature (°C) | Flow Rate ($10^{-6}$ $m^3/s$) | Packing Pressure (MPa) | Holding Time (s) | Cooling Time (s) |
|---|---|---|---|---|---|---|---|
| PS25 | Styron 678E | 25 | 200 | 7.6 | 67 | 15 | 25 |
| PS55 | Styron 678E | 55 | 200 | 7.6 | 67 | 15 | 25 |
| PC50 | Makrolon CD2000 | 50 | 300 | 12.7 | 45 | 10 | 25 |
| No23[a] | Noryl SE-1 | 23 | 320 | 10.2 | 112 | 8 | 39 |
| No90 | Noryl SE-1 | 90 | 320 | 10.2 | 112 | 8 | 39 |

[a] Specimens of this series were annealed for 1 h at 90°C, resulting in series No23 + .

- As a consequence of the viscoelastic nature of plastics, both creep (i) and relaxation (ii) phenomena appear.

(i) After layer removal, the resulting curvature of a specimen increases in time, due to creep (1), obviously leading to erroneous stress values. This phenomenon was also encountered in this study. Therefore, the deflection was always measured within 6 min after layer removal.

(ii) Relaxation of stresses is of minor importance. According to Matsuoka (16), at temperatures far below $T_g$, the stress relaxation modulus $E(t)$, i.e., the reciprocal ratio of a constant strain and the resulting time-dependent stress, can be approximated by

$$E(t) = E_0^*(t/t_0)^{-n} \tag{2}$$

in which $E_0$ and $t_0$ are constants, $t$ is time and $n$ is about 0.02. For example, between 1 day and 10 days the stress relaxation is about 5%. Stress distributions obtained after 1 day and 83 days after the quenching of compression-molded PC plates from 160°C to 23°C revealed no significant decrease in stress. This means that stress relaxation for PC can be neglected for the observed time interval. For the polyphenylene ether/high-impact polystyrene blend, similar results were found by Siegmann, *et al.* (14).

**Table 3. Reproductibility of Measured Deflection.**

| Series No23 Specimen Number | Removed Layer Thickness (μm) | Deflection of Segment (μm) 1 | 3 |
|---|---|---|---|
| 1 | 80 | −13.0 | −8.5 |
| 2 | 80 | −13.1 | −8.2 |
| 3 | 80 | −12.0 | −8.1 |
| 4 | 80 | −13.5 | −8.8 |

| Series No90 Specimen Number | Removed Layer Thickness (μm) | Deflection of Segment (μm) 1 | 3 |
|---|---|---|---|
| 1 | 300 | 64 | 75 |
| 2 | 300 | 65 | 76 |
| 3 | 300 | 66 | 78 |

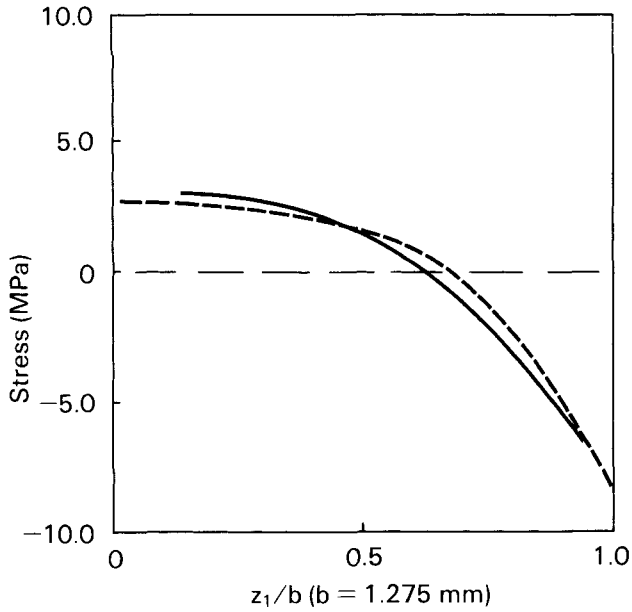


*Fig. 4. Stress distributions of free-quenched compression-molded PS plates. Solid line: results of the present investigation. Dashed line: results of Isayev (12). Position $z_1/b = 0$: original center plane of specimen. Position $z_1/b = 1$: original surface plane of specimen.*

## CURVATURE-STRESS CONVERSION

Stresses were calculated from the curvatures according to the following stress equation:

$$\sigma_x(z_1) = \frac{-E}{6(1-\nu)}\left\{(z_1+b)^2\frac{d\kappa_x(z_1)}{dz_1} + 4(z_1+b)\kappa_x(z_1) - 2\int_{z_1}^{b}\kappa_x(z)\,dz\right\} \tag{3}$$

*Equation 3* was derived from the Treuting and Read relation (15), assuming that the curvature perpendicular to the length direction of the specimen is of the same order as in the length direction. $\sigma_x(z_1)$ is the stress in the length direction $x$ at position $z_1$ measured from the initial center plane of the specimen with initial specimen surfaces located at $z_1 = +/-b$. $E$ is the flexural modulus (see *Table 1*), $\nu$ is Poisson's ratio (taken here to be 0.33 for all materials), while $\kappa$ is the curvature, calculated from *Eq 1*.

A series of curvature data points obtained from one segment were fitted by linear regression with one sixth order polynomial, and subsequently the stress distribution was calculated using *Eq 3*.

In principle, the method of Treuting and Read (15) is applicable to linear elastic materials with isotropic elastic constants. However, the modulus of injection-molded polymers varies over the specimen thickness as a result of molecular orientation distribution. It has been shown that this variation has only a minor influence on the calculated stress distribution (17).

For the reasons mentioned above, the results obtained with *Eq 3* should be regarded as semi-quantitative. Nevertheless, a good indication of the level and distribution of thermal stresses is obtained, which is especially valuable in comparisons, i.e., when determining the stress distributions at different positions along the flow path within one specimen, as is done in this study.

## RESULTS AND DISCUSSION

The results are presented in two parts. The first part describes the stress distributions in injection-molded specimens obtained with different mold temperatures. For this purpose the stress distribution in segment 2 (see *Fig. 3*) was determined. Secondly, the stress distributions along the flow path in relation to different mold-pressure histories are presented. For this purpose, stress distributions in segment 1 and 3 (see *Fig. 3*, with segment 1 nearest to the gate) were determined. The influence of the mold temperatures on the thermal stress distribution was investigated for series PS25, PS55, No23, and No90 (*Table 2*).

As a typical example, a series of deflection profiles of a PS55 specimen is shown in *Fig. 5*. These profiles were measured along the flow path as a function of the dimensionless coordinate $z_1/b$ ($z_1$ is taken from the initial center plane and $b$ is half the thickness of the specimen). The horizontal and vertical axes represent the distance along the flow path and the measured deflection, respectively. Note the different scales of the measured deflections.

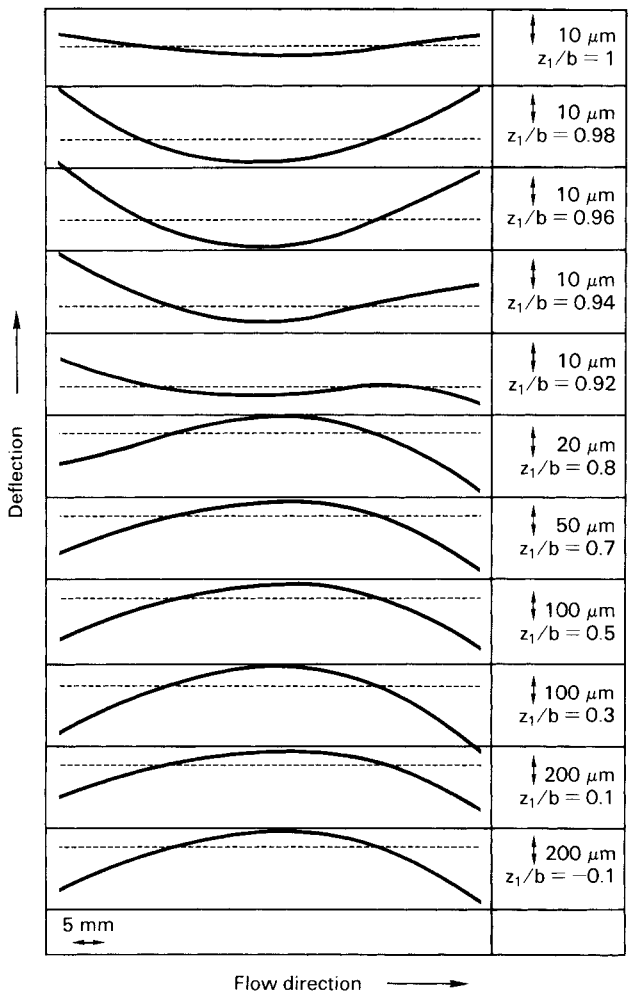


*Fig. 5. Survey of deflection profiles of series PS55. Dashed line: reference line at arbitrary position.*

The upper profile represents the flatness of the original specimen. As can be seen, any initial warpage in the specimens is relatively small compared to changes in deflection by successive layer removals. With the increasing thickness of the removed layer, the sign of the segment 2 deflection with respect to the deflection of the original specimen changes from zero (the deflection of the original specimen is defined as zero) to negative (convex) and then from negative to positive (concave). This means that tensile stresses are present at the surface. The asymmetry of the deflection profiles implies that stresses vary along the flow path.

From these deflection profiles, the curvature halfway along the flow path (segment 2 in *Fig. 3*) was determined, and the corresponding stress was calculated with the aid of *Eq 3*.

For series PS25, No23, and No90 the same procedure was followed. The curvature of segment 2 as a function of the dimensionless coordinate $z_1/b$ is shown for the No and PS series in *Figs. 6a* and *7a*, respectively. The corresponding stress distributions are shown in *Figs. 6b* and *7b*, respectively. From *Fig. 6b* it can be seen that half the cross-section of the specimen (from $z_1/b = 1$ to $z_1/b = 0$) can be subdivided into three regions: a surface region and a core region with tensile stresses and an intermediate region with compressive stresses. With increasing mold temperature, the stress profiles of the No series reveal a reduction of the tensile stresses in

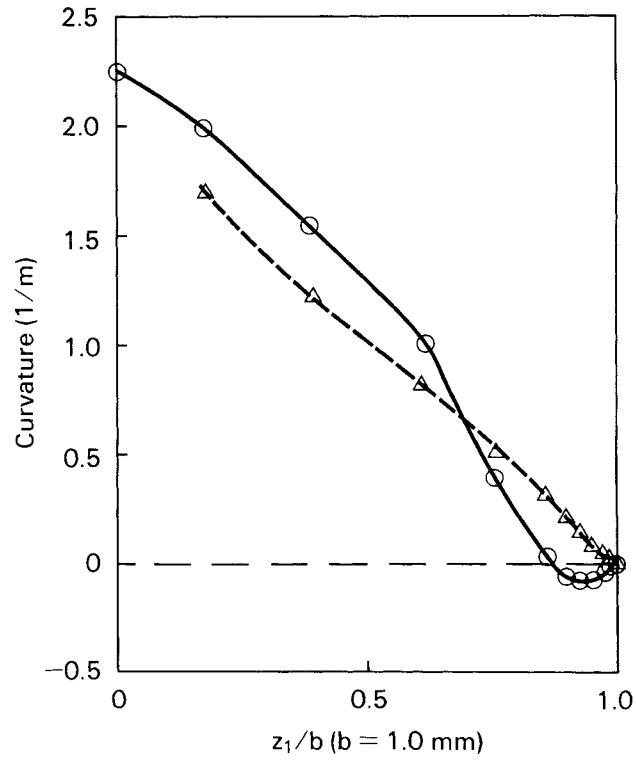


*Fig. 6a. Curvature of segment 2 as function of dimensionless coordinate $z_1/b$. Solid line: series No23. ○: data point. Dashed line: series No90. △: data point.*

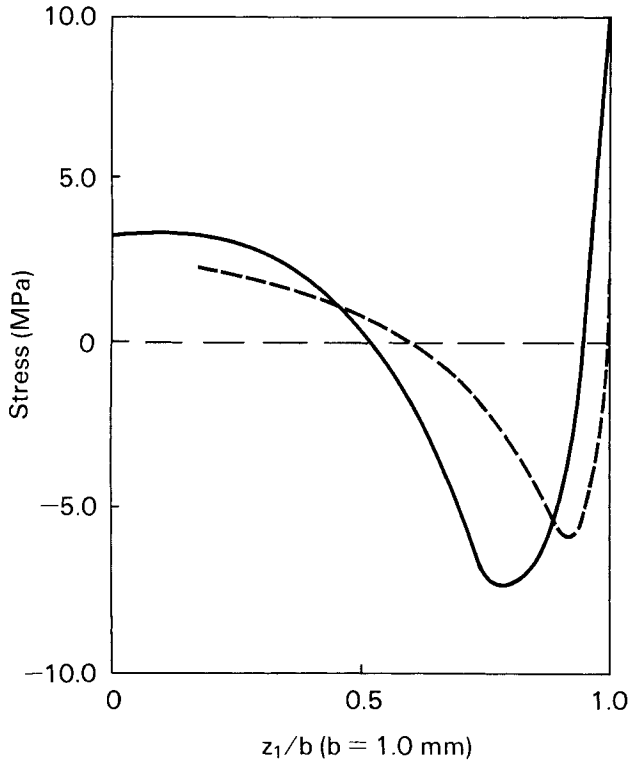


*Fig. 6b. Stress distribution for segment 2. Solid line: series No23. Dashed line: series No90.*

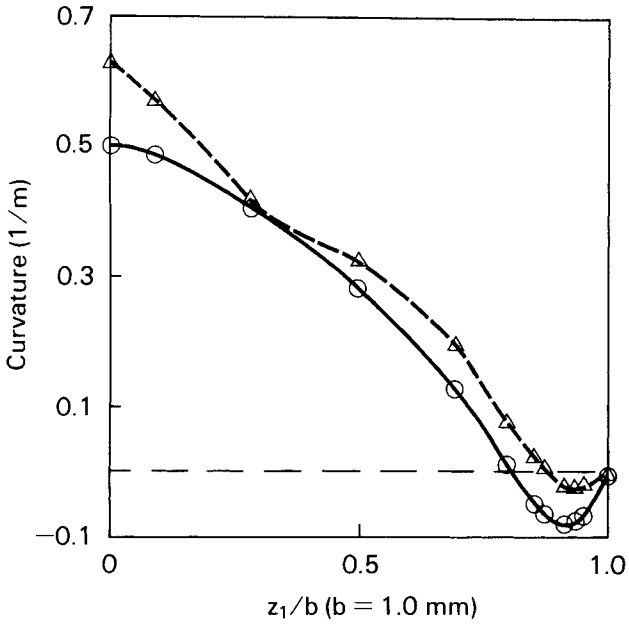


*Fig. 7a. Curvature of segment 2 as a function of dimensionless coordinate $z_1/b$. Solid line: series PS25. ○: data point. Dashed line: series PS55. △: data point.*

both surface and core regions, while at the same time the intermediate compressive stress region clearly shifts to the surface. Overall, increasing mold temperature leads to a lower stress level. This is in agreement with the results of Siegmann, *et al.* (14).

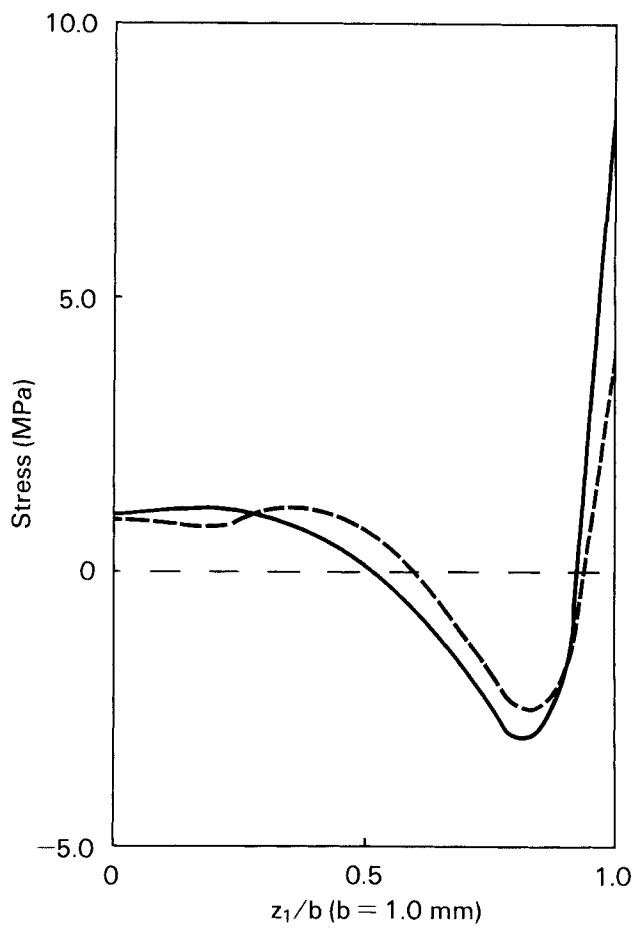


*Fig. 7b. Stress distribution for segment 2. Solid line: series PS25. Dashed line: series PS55.*

The shift of the intermediate region can be explained qualitatively when considering the cooling process in the mold. In the literature (5, 8, 10) the total thermal stress distribution is regarded as the sum of a constrained quench component and a partially frozen-in pressure component. In more detail, in an injection-molding cycle at least four phases can be distinguished: filling phase, packing phase, holding phase, and cooling phase, leading to the formation of the three-region stress distribution.

In the filling phase the mold is filled volumetrically. No significant pressure is present. During this phase solidification starts and includes the build-up of thermal stresses in the surface region. These stresses are due to interaction with the mold wall. This is one of the major differences from a free-quench experiment where during solidification of the surface layers no significant stress is developed.

During the packing phase a high mold pressure is built up. Next, in the holding phase, this pressure is maintained to compensate for shrinkage due to thermal contraction. This high pressure, present during the packing and holding phase, will be partially frozen in and will lead to additional compressive stresses in the intermediate region.

During the cooling phase, the pressure in the mold is substantially lowered. Roughly speaking, layers solidified during this phase are found in the core region. When the mold temperature is lowered, this cooling process is accelerated, shifting the zone (intermediate region) which solidifies during the packing and holding phase, towards the core (*Fig. 7b*).

Mold temperature has less effect on the stress profiles for the PS series than it has for the No series. Only the surface tensile stress is significantly lower for the higher mold temperature. Obviously, the smaller range in mold temperatures, compared with the No series, plays a role.

Annealing procedures to reduce thermal stresses in injection-molded products are well known (3). In this study, No23 specimens were annealed for one hour at 90°C, resulting in series No23 + . The curvature profiles and stress distributions of the No23 + specimens together with the original ones (i.e., from the unannealed specimens) are shown in *Figs. 8a* and *8b*, respectively. It can be seen that the overall stress level is significantly reduced, while the stress pattern is not affected.

The influence of the mold-pressure history on the thermal stress distribution along the flow path was investigated for series PS55, No23, and PC50. For these series, the cavity pressures as a function of time during the injection-molding cycle are shown in *Figs. 9a, 9b* and *9c*, respectively. Each figure shows two pressure profiles, i.e., pressures recorded at points P3 and P4 (indicated in *Fig. 1*).

For the PS55 series, there is a marked difference between the pressure profiles at the beginning and at the end of the flow path. The most striking differences can be described in terms of the pressure decay rate, as used by Titomanlio, *et al.* (8). With this parameter, the pressure decrease during the holding and cooling phases can be described. For

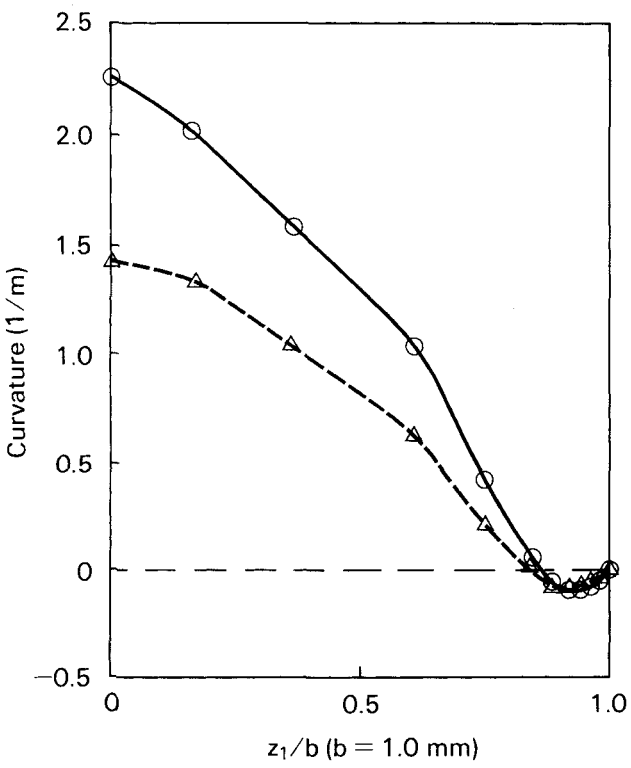


*Fig. 8a. Curvature of segment 2 as a function of dimensionless coordinate $z_1/b$. Solid line: series No23. ○: data point. Dashed line: series No23 + . △: data point.*

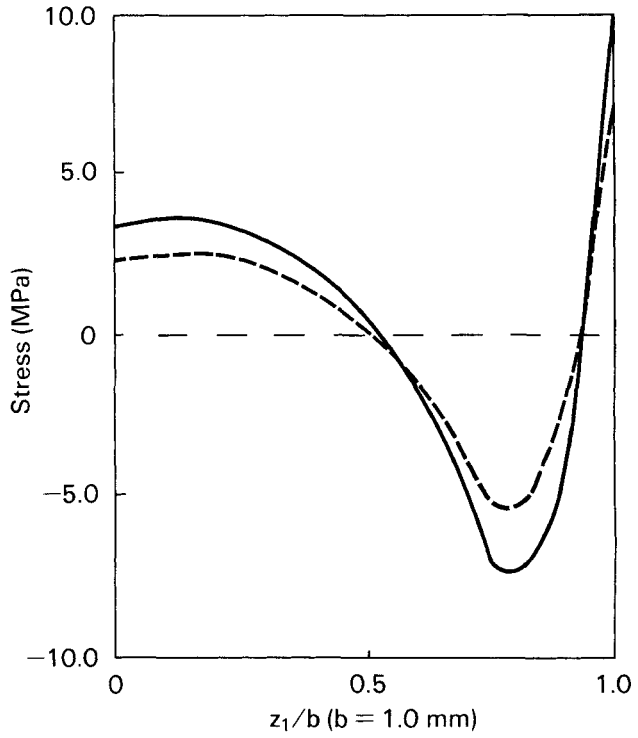


*Fig. 8b. Stress distribution for segment 2. Solid line: series No23. Dashed line: series No23 + .*

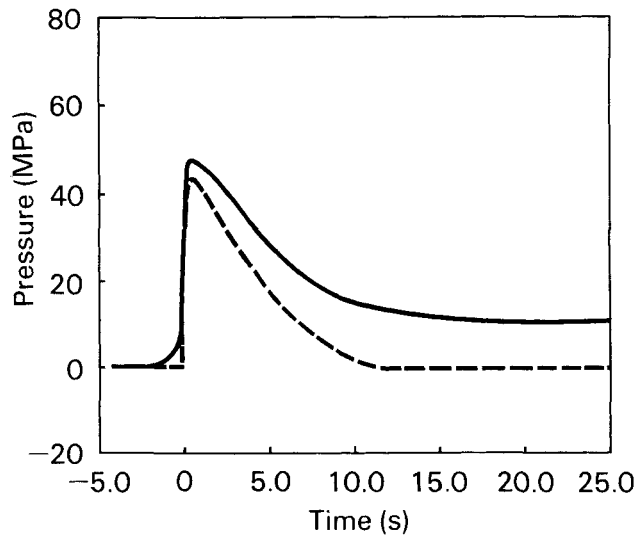


*Fig. 9a. Pressure profiles for series PS55. Solid line: pressure at P3. Dashed line: pressure at P4.*

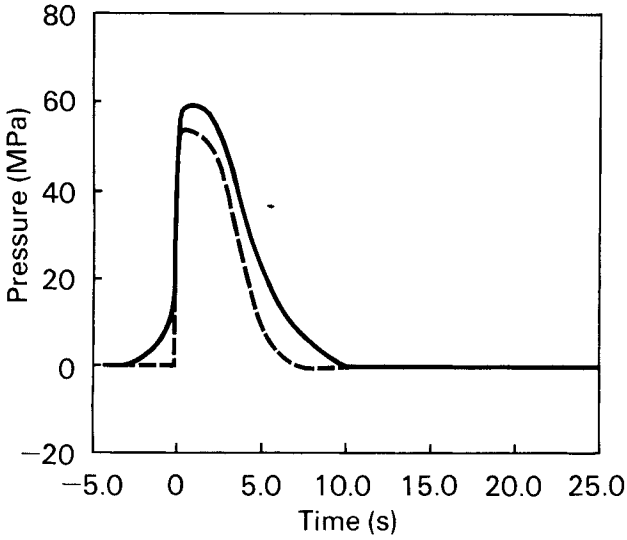


*Fig. 9b. Pressure profiles for series No23. Solid line: pressure at P3. Dashed line: pressure at P4.*

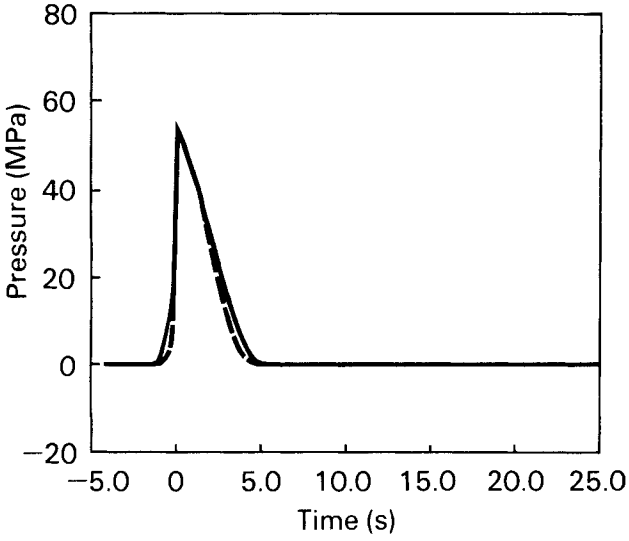


*Fig. 9c. Pressure profiles for series PC50. Solid line: pressure at P3. Dashed line: pressure at P4.*

the PS55 series, this rate is highest at the end of the flow path. Moreover, for this series, some overpacking can be observed at the beginning of the flow path.

No significant difference in the pressure decay rates is detected for the PC50 series, while this rate difference in the No23 series is somewhere in between the PS55 and PC50 series.

The curvature as a function of the dimensionless coordinate $z_1/b$ at the beginning and at the end of the flow path for the three series is shown in *Figs. 10a*, *11a*, and *12a*, respectively. The corresponding stress profiles are shown in *Figs. 10b*, *11b*, and *12b*, respectively. The differences in the curvatures and stress profiles at the beginning and at the end of the flow path agree quite well with the measured differences in decay rate.

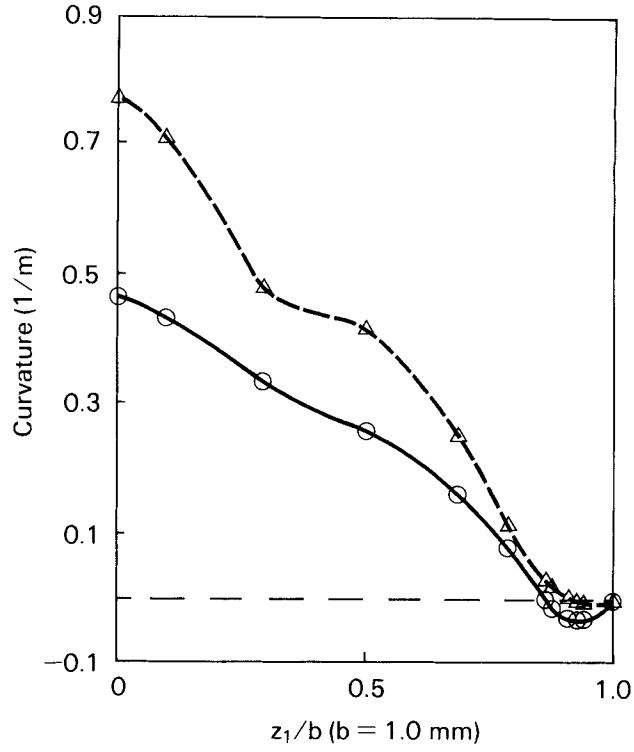


*Fig. 10a. Curvature as a function of dimensionless coordinate $z_1/b$ for series PS55. Solid line: beginning of flow path (segment 1). ○: data point. Dashed line: end of flow path (segment 3). △: data point.*

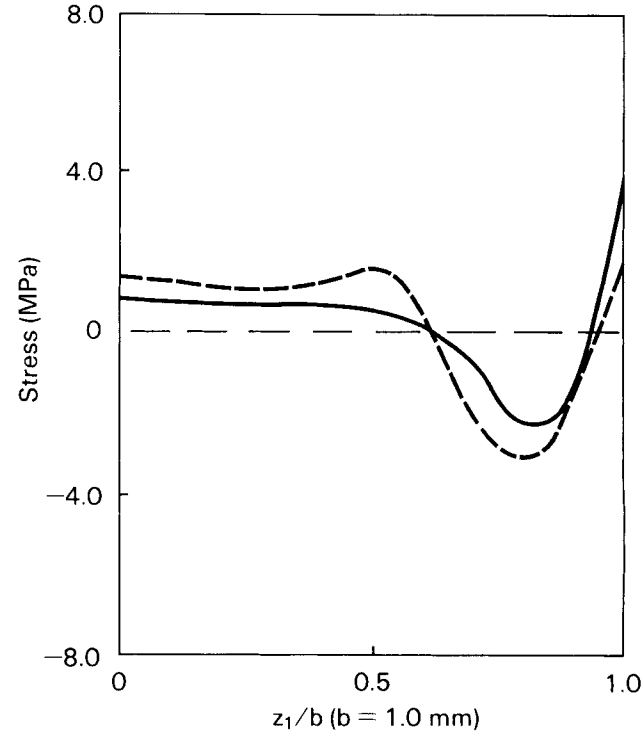


*Fig. 10b. Stress distribution for series PS55. Solid line: beginning of flow path (segment 1). Dashed line: end of flow path (segment 3).*

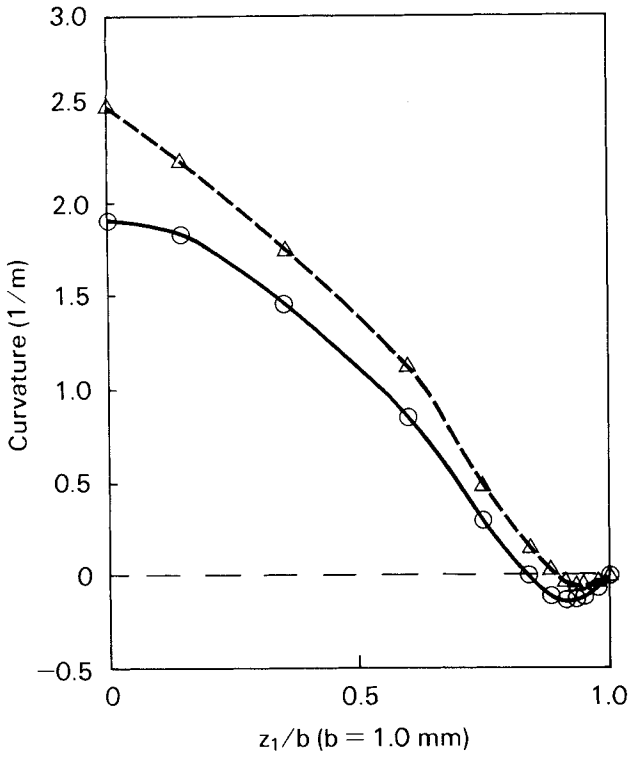


*Fig. 11a. Curvature as a function of dimensionless coordinate $z_1/b$ for series No23. Solid line: beginning of flow path (segment 1). ○: data point. Dashed line: end of flow path (segment 3). △: data point.*

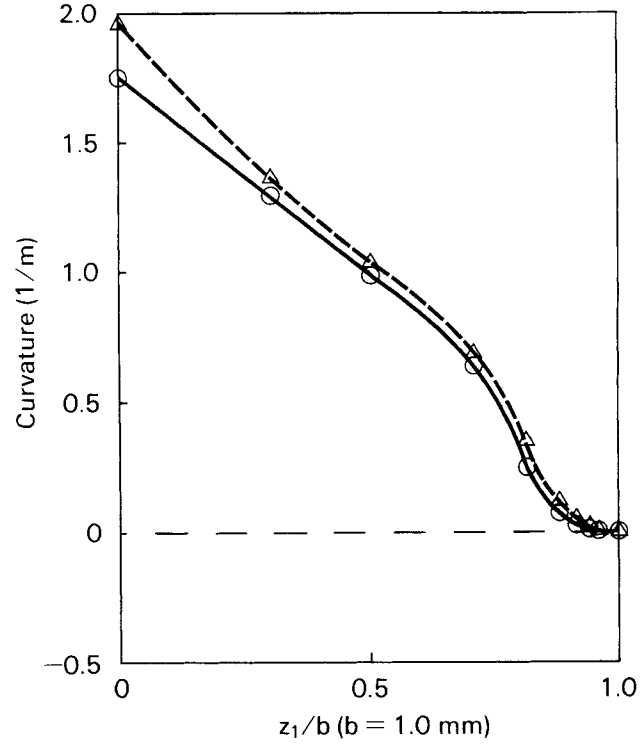


*Fig. 12a. Curvature as a function of dimensionless coordinate $z_1/b$ for series PC50. Solid line: beginning of flow path (segment 1). ○: data point. Dashed line: end of flow path (segment 3). △: data point.*

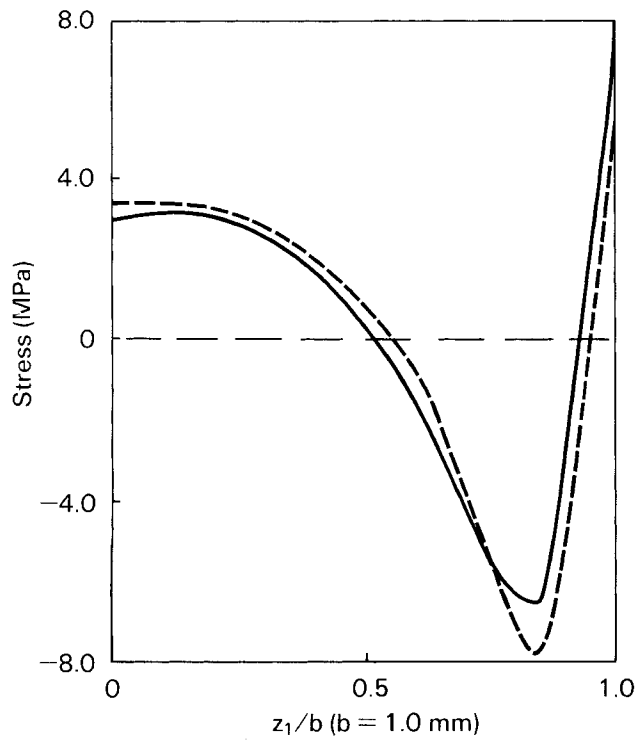


*Fig. 11b. Stress distribution for series No23. Solid line: beginning of flow path (segment 1). Dashed line: end of flow path (segment 3).*

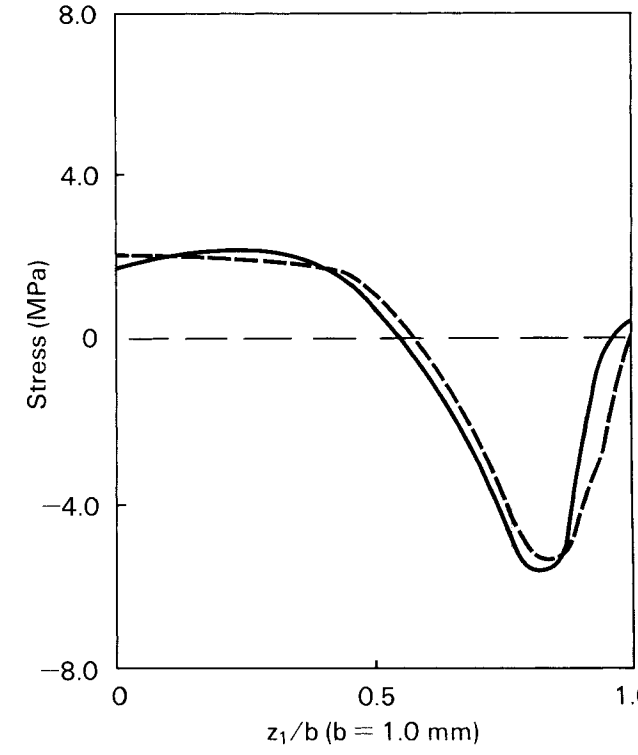


*Fig. 12b. Stress distribution for series PC50. Solid line: beginning of flow path (segment 1). Dashed line: end of flow path (segment 3).*

The PS55 series, with its marked difference in pressure history, also shows large differences in stress distribution (up to a factor of 2). From *Fig 10b* it can be seen that:

- Tensile stresses in the surface region are higher at the beginning of the flow path.
- Compressive stresses in the intermediate region are lower at the beginning of the flow path.
- Tensile stresses in the core region are lower at the beginning of the flow path.

When one assumes that the thermal conditions along the flow path are the same, all observations above can be explained by the influence of the pressure decay rate (8). For the No23 series, the difference in the levels of the surface tensile stresses at the beginning and at the end of the flow path is most striking. The other differences between the stress distributions are small but significant (see *Table 3*) and are in agreement with the observations for series PS55. For the PC50 series no effect could be detected, consistent with the identical pressure profiles at the beginning and at the end of the flow path.

To summarize, a lower pressure decay rate results in a lower overall thermal stress level. However, the stress at the surface becomes higher, which means a higher susceptibility to environmental stress cracking.

## CONCLUSIONS

A modified layer-removal method allows the measurement of the thermal stress distribution along the flow path of an injection-molded flat plate.

The advantages of the presented semi-quantitative method compared with existing methods include:

- Its sensitivity to stress variations along the flow path. By measuring the deflection profile along the flow path after successive layer removals, a survey can be composed (as in *Fig. 5*). From this survey it can easily be deduced, for example, whether or not tensile stresses are present at the surface.
- Stress distributions obtained from a single specimen, thereby eliminating specimen-to-specimen variations and manipulation errors.

In general, the flat-plate cross-section shows up a three-region stress distribution with a tensile stress region both at the surface and in the core of the flat plate and an intermediate region with compressive stresses. Increasing mold temperature results in a decreasing overall stress level, while the compressive stress region shifts to the surface. An annealing treatment significantly reduces the overall stress level, without affecting the stress pattern. The stress distributions vary with distance along the flow path as a consequence of the variation in the pressure history in the flow direction. The various features of the stress profiles can be explained with the aid of the pressure decay rate in the injection-molding process.

## ACKNOWLEDGMENTS

The authors wish to thank R. Wimberger-Friedl for drawing our attention to the possibilities of the layer-removal method for determining the varying stress distributions in the flow direction of injection-molded plates; W. Zoetelief for his stimulating previous work, which will be reported on in due course, and for writing the computer program for the curvature-stress conversion; and F. P. T. Baaijens, A. J. Ingen Housz, D. Samoy, L. C. E. Struik, and F. W. v. d. Weij for stimulating discussions.

## REFERENCES

1. A. I. Isayev, in *Injection and Compression Molding Fundamentals*, Ch. 3, A. I. Isayev, ed., Marcel Dekker, New York (1987).
2. R. P. Kambour, *J. Polym. Sci.: Macromol. Rev.*, **7**, 1 (1973).
3. A. I. Isayev, in *Encyclopedia of Polymer Science and Engineering*, Vol. 16, p. 747, Wiley & Sons, New York (1989).
4. A. M. Flaman, PhD thesis, Eindhoven University of Technology, The Netherlands (1990).
5. F. P. T. Baaijens, to be published in *Rheol. Acta*, **30**, 284 (1991).
6. L. C. E. Struik, in *Internal Stresses, Dimensional Instabilities and Molecular Orientations in Plastics*, Wiley & Sons, Chichester (1990).
7. R. Wimberger-Friedl and R. D. H. M. Hendriks, *Polymer* **30**, 1143 (1989).
8. G. Titomanlio, V. Drucato, and M. R. Kamal, *Intern. Polym. Process.* **1**, 55 (1987).
9. M. Rezayat, *SPE ANTEC Tech. Papers*, **35**, 341 (1989).
10. L. F. A. Douven, PhD thesis, Eindhoven University of Technology, The Netherlands (1991).
11. W. F. Zoetelief, L. F. A. Douven, and A. J. Ingen Housz, to be published.
12. A. I. Isayev and D. L. Crouthamel, *Polym-Plast. Technol. Eng.*, **22**, 177 (1984).
13. B. Haworth, C. S. Hindle, G. J. Sandilands, and J. R. White, *Plast. Rub. Process. Appl.*, **2**, 59 (1982).
14. A. Siegmann, A. Buchman, and S. Kenig, *Polym. Eng. Sci.*, **22**, 560 (1982).
15. R. G. Treuting and W. T. Read, *J. Appl. Phys.*, **22**, 130 (1951).
16. S. Matsuoka, *Polym. Eng. Sci.*, **21**, 907 (1981).
17. M. W. A. Paterson, J. R. White, *J. Mater. Sci.*, **24**, 3521 (1989).